INTERNATIONAL JOURNAL OF
COASTAL & OFFSHORE ENGINEERING
IJCOE Vol.5/No. 4/Winter 2020 (1-8)

Available online at: www. Ijcoe.org

Detecting shoreline change employing remote sensing images (Case study: Beris Port - east of Chabahar, Iran)

Danial Ghaderi [1], Maryam Rahbani [2*]

[1] Ph.D. student, Faculty of Marine Science and Technology, University of Hormozgan, Bandar Abbas 79131, Iran; danialghaderi.phd@hormozgan.ac.ir
[2] Associate Professor, Faculty of Marine Science and Technology, University of Hormozgan, Bandar Abbas 79131, Iran; maryamrahbani@yahoo.com*

ARTICLE INFO

Article History:
Received: 10 Apr. 2020
Accepted: 25 Jun. 2020

Keywords:
Beris Port
DSAS
remote sensing
shoreline change

ABSTRACT

Coastal areas are one of the most crucial and important area in each country. They are also one the most dynamics area, which undergo significant changes in relatively short periods. Protecting coastlines from erosion and/or sedimentation thus, is one of the most important duties in each country. In this study, shoreline change in the Beris Port - east of Chabahar, Iran, was investigated using remote sensing technique and DSAS tools. Beris Port is located 85 km east of Chabahar, on the Makran coast. Landsat 8 and 5 satellite images were used to detect shoreline change, due to the port's construction date, satellite imagery of 1988, 1990, 2014 and 2019 was used. Using the NSM, SCE, EPR and LRR statistical indexes of the DSAS tool, erosion and accretion rates were calculated in for the area. According to the LRR index, the lowest shoreline change rate is -1.51 m/year and is detected to be to the east of port. The highest rate of shoreline change is 7.44 m/year at the port. According the results, the main reason for this high rate of change is the location of the port, which is in the area perpendicular to its neighborhood coastal area, which causes to trap the current in this area to increase its dynamic activities. Shortly speaking, it was found that the accretion is dominant in port Beris and east of the port is the zone with least amount of accretion.

1. Introduction

Coastal areas are dynamic systems with relatively fragile feature. They are affected by many natural and human changes. The most important natural processes that change coastal morphology are, wave, wind, nearshore current, and tide [1,2]. Besides, human processes like coastal engineering activities could cause massive erosion and accretion on the coastal area. Constricting sea walls and breakwaters are those activities which cause the advancement of the shoreline artificially by land reclamation, and the removal of beach material from the coastline is an aspect of retreating coast [3].

Hence the management of coastal areas requires knowledge of the underlying processes of shoreline variability in the medium, inter-annual and decadal time scales [4]. Coastline change is considered one of the most dynamic processes in coastal area. It has become important to map the coastline change as an input data for coastal hazard assessment. Besides, it should be noted that coastal protection might conflict with current land use and economic development activities [5]. There are many change detection techniques currently in use [6]. Using remote sensing and satellite imagery is one of the low-cost and easy methods in coastline detection [7]. Van and Binh (2008), described an application of satellite remote sensing technology and GIS to detect and analyze the spatial changes as well as quantify the result of shoreline change in Cuu Long estuary. Van Cuong et al (2015) using the Shoreline Video Assessment Method (SVAM) applied by satellite images assessed the conditions of the mangrove forest and mainland coastline of the Kien Giang province. Maiti and Bhattacharya (2009), using remote sensing and satellite imagery, studied 113.5 km of coast adjacent to Bay of Bengal in eastern India, for the time interval of 1973 to 2003 [8]. Do et al (2018) used satellite-derived shorelines of NorthHolland coast. They studied the rate of shoreline change calculating volumes of coastal sediments. Nassar et al (2019) recorded shoreline change along the North Sinai coast in Egypt using

geographic information system and digital shoreline analysis system (DSAS) during the elapsed period from 1989 to 2016 [9].

East of Chabahar coastal zone is an important area, and is used for various activities as transportation, fishing and commercial activities, specifically in Beris port. This port, located in southeast of Iran, 85 km east of Chabahar, is one example of the ports constructed in a crenulate-shaped bay. The construction of Beris Fishery Port was finished in 1994. The port has a basin of 25 ha area [10]. The port is suffering from two mechanisms of sedimentation, that is, sedimentation at the head of the main breakwater and remarkable change of shoreline position at the back of the secondary breakwater [11,9]. In addition, construction of the port caused the coastline undergoes significant changes.

In this research, using satellite images and remote sensing, the shoreline is detected and the rate of shoreline change is calculated using the Digital Shoreline Analysis System (DSAS) technique [12].

2. Materials and methods

2.1 Study area

Area under investigation is located east of Chabahar coast, southeast of Iran, along the northern coasts of the Gulf of Oman. Main focus of this study is on the Beris fishery port at 25.147° N latitude and 61.176° E longitude (Figure 1), This fishing port is located 85 km east of Chabahar [10]. Since the study area is quite long, it was considered to divide it into three adjacent zones of A, B and C, they are shown in Figure 1 as parts A, B and C respectively. Zone A is in the western of the Beris port, Zone B is at the middle and contains Beris port, and Zone C is in the eastern of the port.

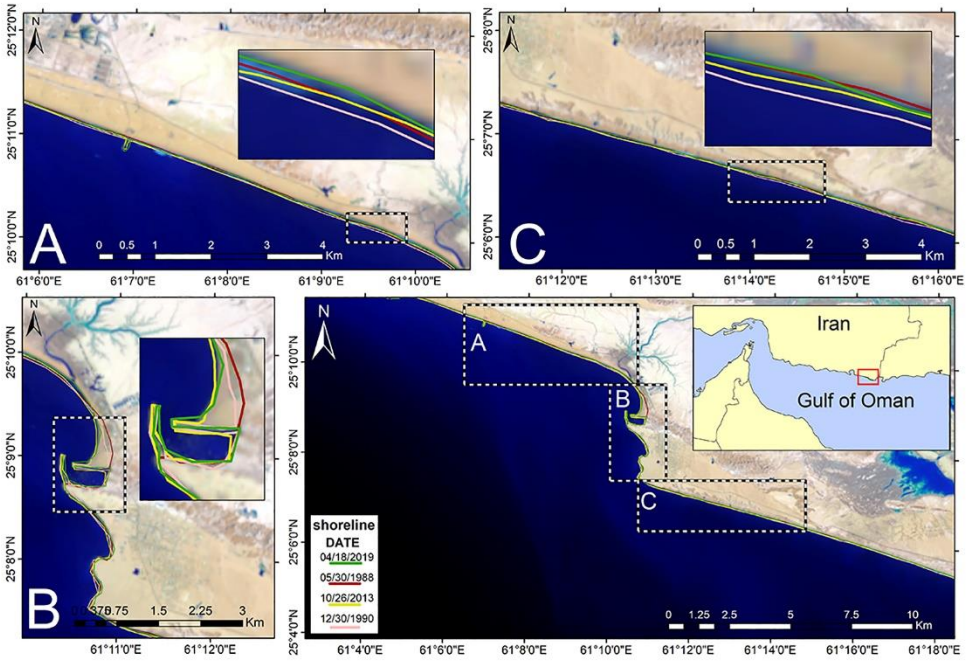

Figure 1: Map of study area in the east of Chabahar- Iran

The area includes approximately 50 km of coastline. This region is adjacent to the Gulf of Oman and is influenced by the Indian Ocean. Tidal condition is mesotidal type and semidiurnal with a range of approximately 1.66 m (Figure 2A). The wind rose of this region indicates domination of wind from the northeast. The average wind speed is about 3.8 m/s and the highest recorded speed is 6.1 m/s (Figure 2B).

According to studies carried out in the Beris Port, the main reason for sediment transport in the area is regional currents. According to literature, areas most affected by sedimentation are the head of the main breakwater and the back of the secondary breakwater [10].

Sayehbani and Ghaderi [13] developing a numerical model of MIKE21, studied the pattern of current and wave around this port. Figure 3 shows the pattern of waves and currents around the Beris port conducted by them. It can be seen that in the back of the main breakwater, the wave height and current velocity are relatively low (sign 2 in left and right side image). However, in the eastern part of the port relative strong current is observable (sign 3 in left side image). They also suggested strong sedimentation in the area which might be detectable by comparing satellite images of different years.

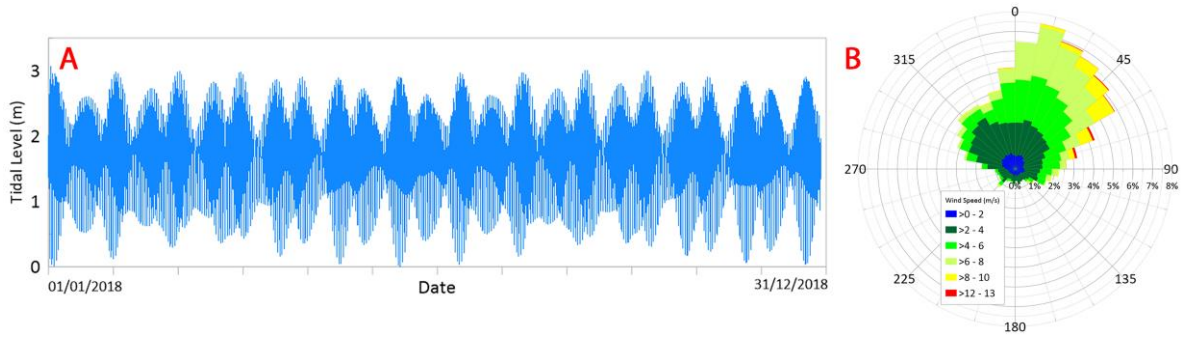

Figure 2: Tidal level (m) in Beris Port from 01/01/2018 – 31/12/2018, taken from National Cartographic Center of Iran (A). Wind rose of the east of Chabahar from 01/01/2018 – 31/12/2018, taken from ECMWF [14] (B)

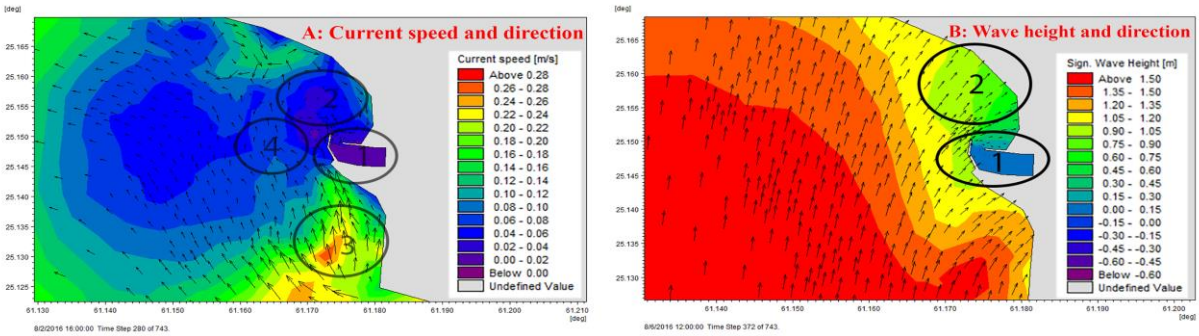

Figure 3: Patterns of wave and current around the Beris port. A) Current speed and direction, B) wave height and direction [13]

2.1 Shoreline detection

2.1.1 Data sources

To monitor shoreline change, georeferenced satellite images from Landsat OLI/TIRS and TM of the years 1988, 1990, 2014 and 2019 were used (Table 1). The logic behind the selection of these years are discussed as follow. Cloud cover causes the loss of important signs in the satellite images. Thus, the main concern for choosing the years was the clarity of the images from clouds. Year 2019 was chosen as the latest coastline records. The closest year (with good clarity images) with at least 5 year interval of the latest change was the year 2014. The first cloud-free image recorded after the construction of the Baris Port was belonged to the year 1990, and the last cloud-free recorded image before the construction of the Port was the year 1988. Landsat satellite imagery with a resolution of 30 meters is the most important tool for investigating shoreline changes [15].

Table 1: Details of data used in this study

Satellite data	Path/Row	Year of acquisition	Resolution (pixel size) (m)	Zone
Landsat 8 OLI/TIRS	156/43	18/04/2019	30	A, B, C
Landsat 8 OLI/TIRS	156/43	22/05/2014	30	A, B, C
Landsat 5 TM	156/43	20/05/1990	30	A, B, C
Landsat 5 TM	156/43	30/05/1988	30	A, B, C

OLI, operational land imager; TIRS, thermal infrared sensor; TM, thematic mapper

2.1.2 Image processing

Image processing involves several steps including geometric, radiometric and atmospheric correction. Using available satellite and aerial imagery, and selection control points in the area, geometric correction is prepared by software ENVI 5.3. Prominent geomorphologic features and river channels where selected as control points. The coordinate system of images has been transformed into Universal Transverse Mercator (UTM). Radiometric and atmospheric correction includes subtraction of the atmospheric contribution, reduction of illumination, viewing angles and terrain effects, and sensor calibration [16,17,18]. These steps are performed using tools in ENVI 5.3 software [7,17,19].

2.1.3 Shoreline Extraction

A sophisticated way to distinguish the border between sea and land is the usage of satellite images with different frequency bonds. In general, water can absorb most near-infrared and mid-infrared radiation. Thus, its reflection is almost zero at these frequencies, while, everything except water are rather reflective. According to this concept, infrared band images can be used as criterion to distinguish the shoreline.

A common method for Landsats image processing, which is also employed by Niya et.al (2013) is the usage of the band ratio [20]. In this method binary-image-1 is generated using the ratio of Band2/Band4 and Band2/Band5. Afterwards, binary-image-2 is developed using the histogram threshold based on band 5. Image-3 is generated by multiplying the two binary images of 1 and 2, in which the deviation between the sea and the land is clearly distinguishable [19,20]. It should be noted that in Landsat 8 the number of bands are different from previous Landsats. That is; bands 2, 4 and 5 are respectively 3, 5, and 6 [21,17]. The final

step involves converting raster images to vector. Afterwards, those modified images are imported to the ArcGIS software to extract the shoreline.

2.2 Shoreline changes assessment

By determining the shoreline variation along transects, changes in the coast and rate of change are measured. For this purpose, a baseline can be created along the shoreline at desired distance, then several transects perpendicular to the baseline would be created with arbitrary distances from one another [22,23]. There are several statistical methods for calculating rate of shoreline change, of which the most common are end-point rate (EPR) and linear-regression rates (LRR) [24]. EPR is simply the rate determined calculating the distance between the oldest and most recent shorelines. LRR is the result of estimating the average rate of changes of shoreline positions over the time [22,12].

In this study, to identify changes in the shoreline by statistical methods, DSAS tool developed by USGS for ArcGIS software is used. There are five steps to use a DSAS tool including: shorelines preparation, baseline creation, transects generation, computation of distances between baseline and shorelines at each transect, and computation of rate of shoreline change (Figure 4) [12]. In this study, in addition to EPR and LRR, SCE and NSM are calculated. The net shoreline movement (NSM) is the distance between the oldest and the youngest shorelines for each transect. The shoreline change envelope (SCE) value represents the greatest distance detected between all the shorelines among all intersects regardless time [12], which means SCE reports a distance in meters. The EPR index is the outcome of dividing the distance of shoreline movement (NSM) by the time elapsed between the oldest and the most recent shoreline [12]. A linear regression rate-of-change statistic can be determined by fitting a least-squares regression line to all shoreline points for a transect. The regression line is placed so that the sum of the squared residuals (determined by squaring the offset distance of each data point from the regression line and adding the squared residuals together) is minimized. The linear regression rate is the slope of the line [12]. Figure 4 shows how these indexes can be calculated. The LRR index has following features: (1) the data can be used irrespective of trend or accuracy, (2) the method is purely computational, (3) the calculation is based on accepted statistical concepts, and (4) the method is easy to employ [25,24].

In this study, the length of shoreline is 48.2 km (according to the measurements of the year 2019), 485 transects are selected with 50 m intervals. This interval value is selected considering the resolution of the images. The coastline is then subdivided into three zones A, B and C (Figure 1), with 184, 132 and 169 transects, respectively. The first transect is located at the western side of zone A, and the last is at the eastern side of zone C. It should be mentioned that 4 transects of zone A, and 18 transects of zone B has been eliminated due to the coastal constructions (Figure 5). It is also necessary to mention that zone B is almost perpendicular to Zones A and C (see Figure 1).

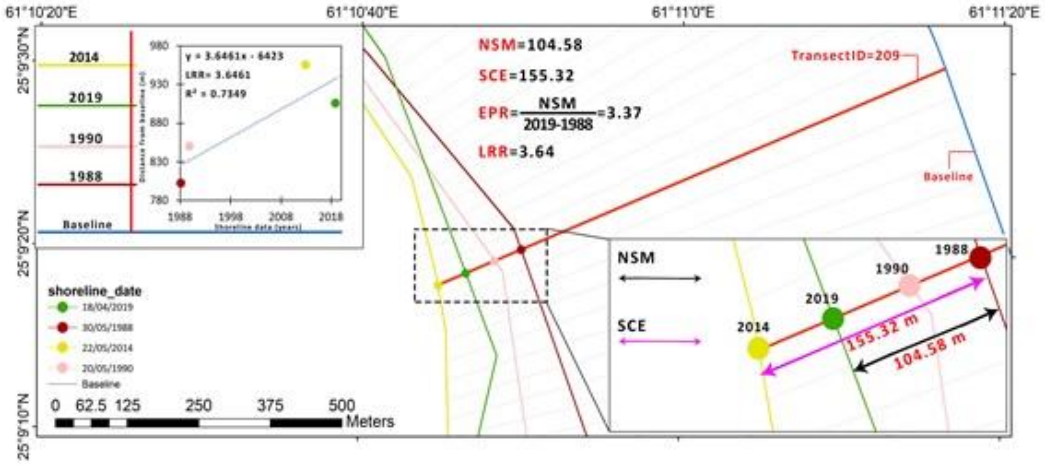

Figure 4: Schematic of the calculation of indexes; NSM, SCE, EPR and LRR in transects 209

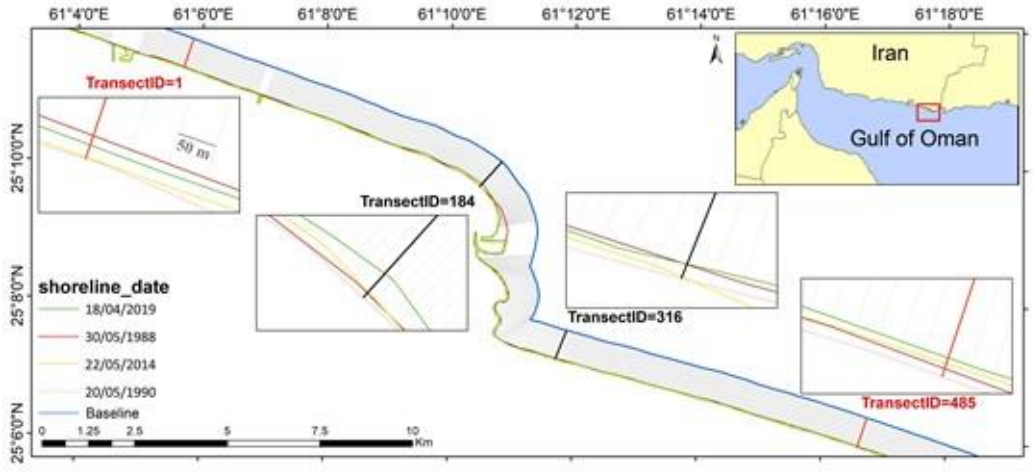

Figure 5: Location of transects, baseline and shoreline for 2019, 2014, 1990 and 1988

3. Results and Discussion

After selecting transects, values of SCE, NSM, EPR, and LRR index are calculated using DSAS tool. Analyzing these indexes, the amount of erosion or accretion in each transect is calculated. Figure 6 shows the shoreline changes from 1988 to 2019 with respect to the two SCE and NSM indexes. The SCE index shows the most changes made regardless data history. Therefore, the SCE index does not show the difference of erosion or accretion, and is always a positive number. As shown in Figure 6, most of the shoreline change occurred west of the Beris Port; areas of significant variation are marked with a dashed square. Due to the characteristic of the SCE index, values close to zero shows minor changes of the shoreline during the period of investigation. During this period the smallest change along the shoreline occurred close to the Beris Port (about 250 m east). The NSM index can indicate the amount of erosion/accretion by evaluating the distance between the oldest and the youngest shorelines. Figure 6 shows that most of the accretion occurred approximately 241 m west of the Beris Port, and the highest erosion occurred at a transect ID 204 (about 89.79 m). By comparing the SCE and NSM index, the type of changes (erosion or accretion) between 1988 and 2019 can be determined.

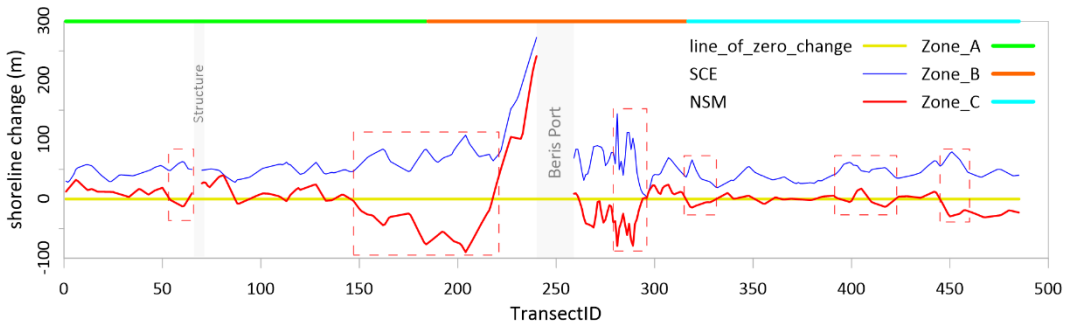

Figure 6: Shoreline change by SCE and NSM index in zone A, B and C during the period 1988 and 2019

The EPR and LRR index can be used to obtain the rate of shoreline changes between 1988 and 2019. Figure 7 shows the annual variation of these two indexes along the shoreline. Generally speaking, the highest and lowest rate of change is observed on the west and east side of the port respectively. There is also aforementioned point of about 250 meters west of the port with the low late of change.

Figure 8 shows the comparison between the two statistical methods of EPR and LRR. Good correlation between EPR and LRR can be observed for zones A and B (Figure 8(a) and 8(b)) with the $R^2 = 0.95$ and 0.96 respectively. In zone C however, weak correlation between the two statistical methods is detected with R2 of 0.61 (Figure 8(c)). One reason for the weak correlation between the two indexes in zone C could be the negligible change between the oldest (1988) and newest (2019) shoreline. It should be noted that it might be considerable variation in shoreline between 1988 and 2019, which is neglected by considering ERP, while LRR index considers the variation between these two years. This can explain the weak result of R2 for Zone C.

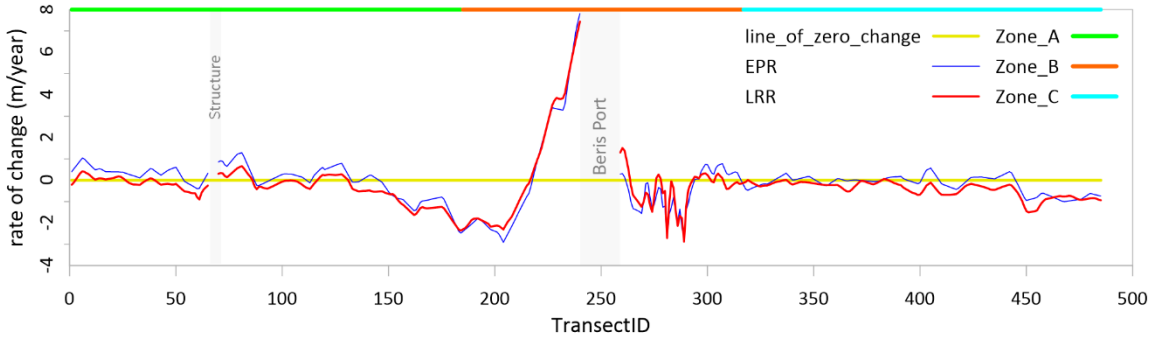

Figure 7: Rate of shoreline change by EPR and LRR index in zone A, B and C during the period from 1988 to 2019

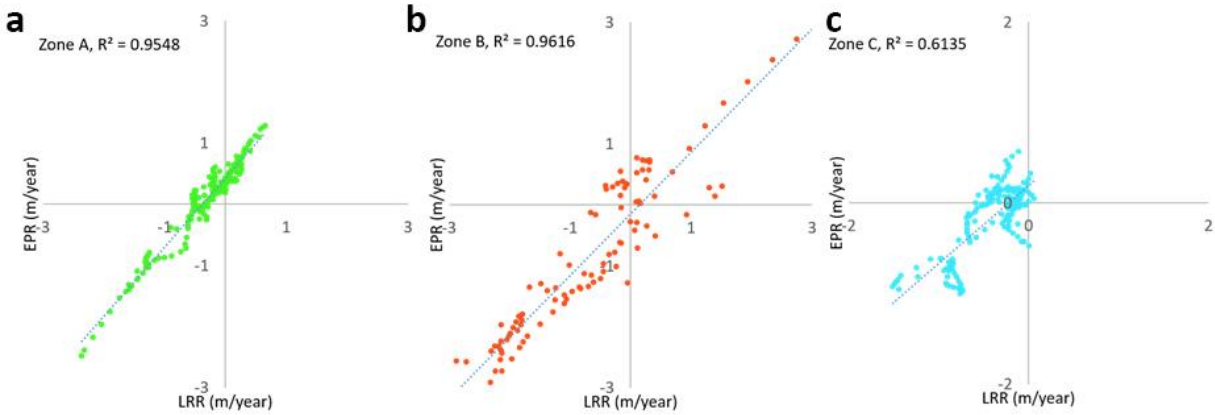

Figure 8: Comparison of shoreline rates (m/year) obtained by different statistical methods (EPR and LRR) in zone A, B and C

Evaluating the results, it was found that LRR index is the most suitable index for describing the erosion and accretion process in all three zones. Table 2 shows the rate of change along the shoreline statistically (m/year) for three zones A, B and C for the duration 1988 to 2019. Figure 9 to 11 show all transects of zone A, B, and C respectively. They are colored according to the LRR value; red means erosion and green means accretion. In the areas near the Beris Port, the maximum erosion rate is 20.36 m and the maximum accretion rate is 0.66 m. Erosion is dominant process in the zone A. On the east side of the structure however, accretion is dominated (Figure 9). Zone B has the highest accretion (7.44 m/year); this is especially evident in the vicinity of western Beris Port (Figure 10). The dominant process in coastline zone C is erosion (Figure 11), but the erosion rate is slower than the other two zones (0.43 m/year in average).

Table 2: Shoreline changes rate (m/year) in three zones A, B and C from 1988 to 2019

Zone	Minimum	Maxim	Average	Standard deviation
A	-2.36	0.66	-0.33	0.60
B	-2.88	7.44	0.058	2.04
C	-1.51	0.06	-0.43	0.35

Figure 9 to 11 are also contain averaged wind speed over the sea, which is presented as a colored area, and a direction. It can be seen that the averaged-speed is about 3.1 to 3.7 m/s in all of the zones, which is in coincidence with results of Figure 2. However, its direction in all three zons is northwest, which is not the same with results presented in Figure 2. This direction of wind can be a factor responsible for circulation observed in Figure 3 in vicinity of Beris Port. This is the area with the highest sedimentation (Figure 10). This means that constructing Beris Port is the main reason for sedimentation in the area. In the zone C (Figure 11) the direction of the current is parallel to the coastline with 3.2 m/s speed. It is therefore, expected uniform erosion or sedimentation along the coast, which can be observed in Figure 11.

It should also be noted that the configuration of coastline zones A and C are almost east-west, while coastline of zone B is almost north-west. This different configuration causes different response of zone B to the dynamic processes such as wind and current. Since this area is perpendicular to the two other Zones, the current could be trapped there and causes circulation as suggested by Sayehbani and Ghaderi (2019). Besides, constructing Beris Port in this zone can be count as another destructive factor for increment in sedimentation and/or erosion there.

According to the ECMWF wind data, the mean annual wind speed in the zone A and B is 3.7 m/s and its predominant direction is southeast (Figure 9,10). The current status of zone A is in the east-west direction. However, near the port of Beris (east of zone A), there is a cycle opposite to the current direction (most erosion occurred in this area). In zone B, due to the Beris port construction, the direction of current is opposite to the main direction in the area (Figure 3A), so this current causes accretion near the port. Zone C has the same wind direction as other zones, but its speed is slightly lower; approximately 3.2 m/s (Figure 11). The

direction of current in this area is also parallel to the coastline.

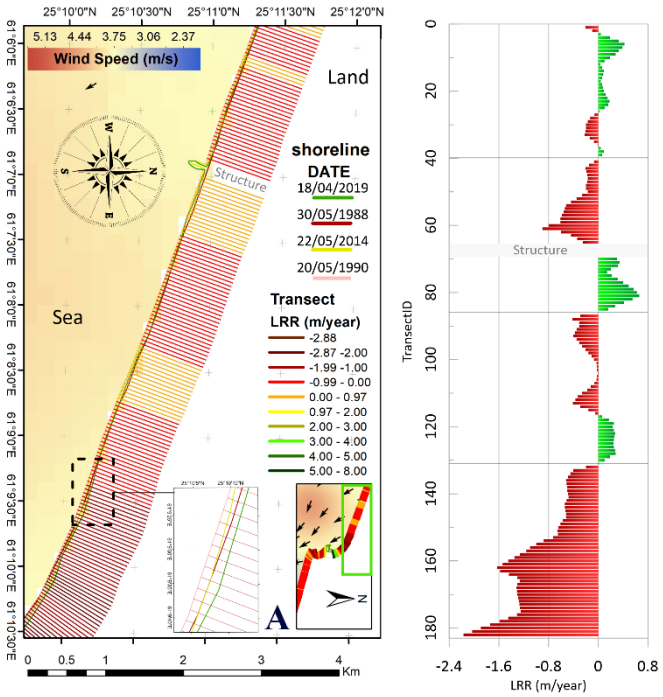

Figure 9: Shoreline evolution between 1988 and 2019 by LRR in zone A. Note: In this figure the dominant wind direction and direction are also shown in the area

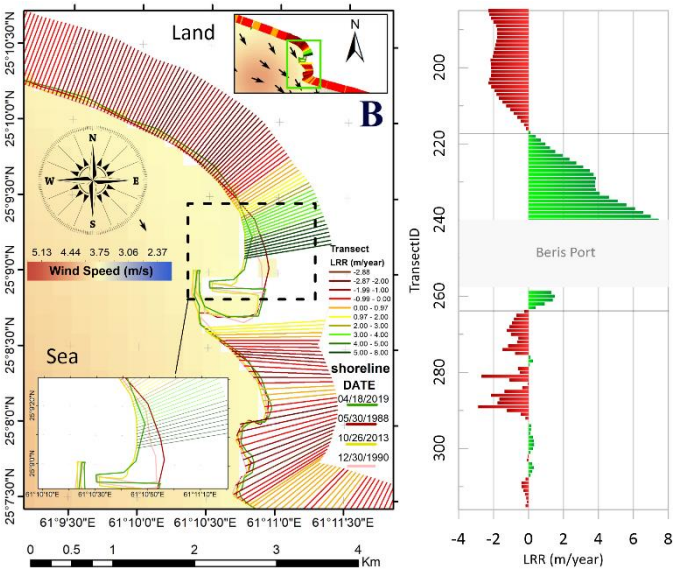

Figure 10: Shoreline evolution between 1988 and 2019 by LRR in zone B. Note: In this figure the dominant wind direction and direction are also shown in the area

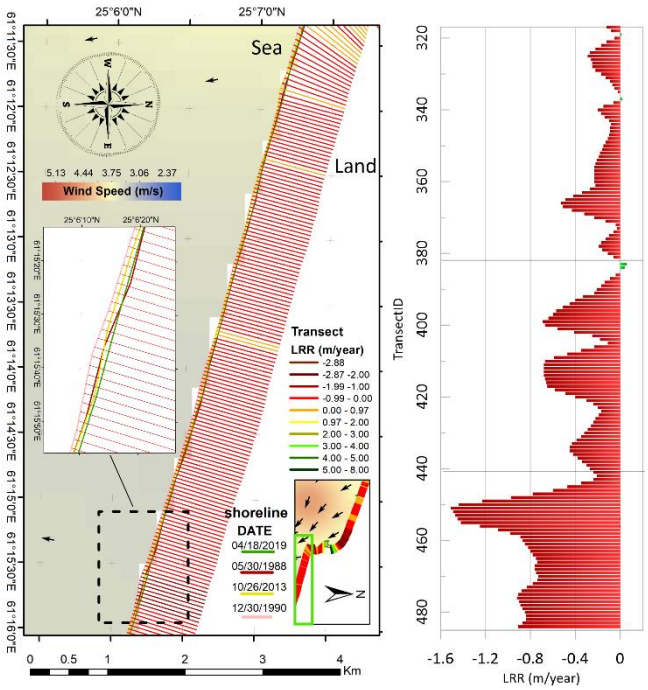

Figure 11: Shoreline evolution between 1988 and 2019 by LRR in zone C. Note: In this figure the dominant wind direction and direction are also shown in the area

4. Conclusion

Images derived from Landsat 8 and 5 of the years 1988, 1990, 2014 and 2019 has been used to assess the rate of erosion/sedimentation along the coastline of Beris east of Chabahar, in Iran. The highest shoreline change (erosion-accretion) was recorded as 7.44 m/year adjacent to the west of the port of Beris and -2.88 m/year at the east of the port (approximately 1500 m from the port of Brice). It was specifically found that the area close to the port of Brice suffers from erosion-accretion rate at most. The direction of the wind, the shape of the coastline, and the pattern of current in the area can be count as the factors responsible for shoreline change. The direction of wind is almost the same in the whole area, while due to the location of Beris port, which its coastline is perpendicular to the adjacent zones, this port is affected by erosion/accretion at most. This can increase the effect of wind and current on this coastline. Also due to the construction of the port, the local current is affected, which can also be accounted as a factor for increasing the rate of change in shoreline. In the western part of the port; after shoreline erosion, the sedimentation took place at the vicinity of the secondary breakwater of the port. Also, in the eastern part erosion occurs due to the shape of the coastline and high current velocity.

5. References

1- Parthasarathy K, Deka PC (2019) *Remote sensing and GIS application in assessment of coastal vulnerability and shoreline changes*: a review. ISH J. Hydraul. Eng., 1-13.

2- Van TT, Binh T. T (2008) *Shoreline change detection to serve sustainable management of coastal zone in Cuu Long Estuary*. Paper presented at the

International Symposium on Geoinformatics for Spatial Infrastructure Development in Earth and Allied Sciences.

3- Bird ECF, Ongkosongo OS (1980) *Environmental changes on the coasts of Indonesia*: UNU.

4- Oost A, Hoekstra P, Wiersma A, Flemming B, Lammerts E, Pejrup M, Bartholdy J (2012), *Barrier island management: Lessons from the past and directions for the future*. Ocean Coast Manage, 68, 18-38.

5- Van Cuong C, Russell M, Brown S, & Dart P (2015) *Using Shoreline Video Assessment for coastal planning and restoration in the context of climate change in Kien Giang, Vietnam*. Ocean Sci J, 50(2), 413-432.

6- Marfai MA, Almohammad H, Dey S, Susanto B, King L (2008) *Coastal dynamic and shoreline mapping: multi-sources spatial data analysis in Semarang Indonesia*. Environ Monit Assess, 142(1-3), 297-308.

7- Do AT, de Vries S, Stive MJ (2018) *The Estimation and Evaluation of Shoreline Locations, Shoreline-Change Rates, and Coastal Volume Changes Derived from Landsat Images*. J Coastal Res.

8- Maiti S, Bhattacharya AK (2009) *Shoreline change analysis and its application to prediction: A remote sensing and statistics based approach*. Mar Geol, 257(1-4), 11-23.

9- Nassar K, Mahmod W E, Fath H, Masria A, Nadaoka K, Negm A (2019) *Shoreline change detection using DSAS technique: Case of North Sinai coast, Egypt*. Mar Georesour Geotechnol, 37(1), 81-95.

10-Ardani S, Soltanpour M (2015) *Modelling of sediment transport in Beris fishery port*. CEIJ, 48(1), 69-82.

11- Hajivalie F, Soltanpour M (2007) *Beris fishing port, interfering in the equilibrium shape of a bay*. In Coastal Engineering 2006: (In 5 Volumes) (pp. 3843-3850): World Scientific.

12- Thieler ER, Himmelstoss EA, Zichichi JL, Ergul A (2009) *The Digital Shoreline Analysis System (DSAS) version 4.0-an ArcGIS extension for calculating shoreline change (2331-1258).* Retrieved from

13- Sayehbani M, Ghaderi D (2019) *Numerical Modeling of Wave and Current Patterns of Beris Port in East of Chabahar-Iran*. IJCOE, 3, 21-29.

14- Berrisford P, Dee D, Poli P, et al (2011) *The ERA-Interim archive, version 2.0*.

15- Blodget H, Taylor P, Roark J (1991) *Shoreline changes along the Rosetta-Nile Promontory: Monitoring with satellite observations*. Mar Geol, 99(1-2), 67-77.

16- Lillesand T, Kiefer RW, Chipman J (2015) *Remote sensing and image interpretation*; John Wiley & Sons.

17- Louati M, Saïdi H, Zargouni F (2015) *Shoreline change assessment using remote sensing and GIS techniques: a case study of the Medjerda delta coast*, Tunisia. Arabian J Geosci, 8(6), 4239-4255.

18- Mather PM, Koch M (2011) *Computer processing of remotely-sensed images: an introduction*; John Wiley & Sons.

19- Masria A, Nadaoka K, Negm A, Iskander M (2015) *Detection of shoreline and land cover changes around Rosetta promontory, Egypt, based on remote sensing analysis*. Land, 4(1), 216-230.

20- Niya AK, Alesheikh AA, Soltanpor M, Kheirkhahzarkesh MM (2013) *Shoreline change mapping using remote sensing and GIS*. IJRSA, 3(3), 102-107.

21- Kuleli T (2010) *Quantitative analysis of shoreline changes at the Mediterranean Coast in Turkey*. Environ Monit Assess, 167(1-4), 387-397.

22- Chand P, Acharya P (2010) *Shoreline change and sea level rise along coast of Bhitarkanika wildlife sanctuary, Orissa: an analytical approach of remote sensing and statistical techniques*. IJGGS, 1(3), 436.

23- Emran A, Rob MA, Kabir MH, Islam MN (2016) *Modeling spatio-temporal shoreline and areal dynamics of coastal island using geospatial technique*. MESE, 2(1), 4.

24- Dolan R, Fenster MS, Holme SJ (1991) *Temporal analysis of shoreline recession and accretion*. J Coastal Res, 723-744.

25- Crowell M, Douglas BC, Leatherman SP (1997) *On forecasting future US shoreline positions: a test of algorithms*. J Coastal Res, 1245-1255.